applied sciences

MDPI

Article

Optimizing CNT Loading in Antimicrobial Composites for Urinary Tract Application

Marisa Gomes [1], Luciana C. Gomes [1], Rita Teixeira-Santos [1], Manuel F. R. Pereira [2], Olívia S. G. P. Soares [2,*] and Filipe J. Mergulhão [1,*]

[1] LEPABE—Laboratory for Process Engineering, Environment, Biotechnology and Energy, Faculty of Engineering, University of Porto, Rua Dr. Roberto Frias, 4200-465 Porto, Portugal; marisagomes@fe.up.pt (M.G.); luciana.gomes@fe.up.pt (L.C.G.); ritadtsantos@fe.up.pt (R.T.-S.)

[2] Associate Laboratory LSRE-LCM, Department of Chemical Engineering, Faculty of Engineering, University of Porto, Rua Dr. Roberto Frias, 4200-465 Porto, Portugal; fpereira@fe.up.pt

* Correspondence: salome.soares@fe.up.pt (O.S.G.P.S.); filipem@fe.up.pt (F.J.M.); Tel.: +351-225081779 (O.S.G.P.S.); +351-225081556 (F.J.M.)

Featured Application: Carbon nanotube composites produced in the scope of this work can potentially be used as a starting point for designing urinary tract devices with inherent antibiofilm activity.

Abstract: Several methodologies have been implemented with the intent of preventing or reducing the formation of biofilms on indwelling urinary devices. The use of carbon nanotubes (CNTs) in the biomedical field has been increasing, particularly in the production of antimicrobial and antifouling coatings. Despite their proven antimicrobial properties, their use as coating materials for urinary tract devices (UTDs) is still poorly documented. In the present work, CNT/poly(dimethylsiloxane) (PDMS) composite materials containing different CNT loadings were prepared and further tested against *Escherichia coli* under conditions prevailing in UTDs. Besides CNT loading optimization, textural modifications were also introduced on the surface of CNTs to improve the antibiofilm properties of the final composites. Material characterization included the textural evaluation of CNTs and the assessment of surface morphology by scanning electron microscopy, while the surface hydrophobicity was determined by contact angle measurements. Biofilm analysis was performed by determining the number of culturable and total cells and by confocal laser scanning microscopy. Results revealed that, by filling the PDMS matrix with 3 wt% CNT loading, a significant reduction in cell culturability (39%) can be achieved compared to PDMS. Additionally, the textural modifications induced by ball-milling treatment proved to be effective on the inhibition of biofilm formation, reducing the amount of biofilm per surface area, biofilm thickness and surface coverage in 31, 47 and 27%, respectively (compared to surfaces where CNTs were not ball-milled).

Keywords: carbon nanotube composites; poly(dimethylsiloxane); *Escherichia coli*; antibiofilm activity; urinary tract devices

Citation: Gomes, M.; Gomes, L.C.; Teixeira-Santos, R.; Pereira, M.F.R.; Soares, O.S.G.P.; Mergulhão, F.J. Optimizing CNT Loading in Antimicrobial Composites for Urinary Tract Application. *Appl. Sci.* **2021**, *11*, 4038. https://doi.org/10.3390/app11094038

Academic Editor: Elzbieta Pach

Received: 17 March 2021
Accepted: 26 April 2021
Published: 29 April 2021

1. Introduction

Urinary tract devices (UTDs), namely urinary catheters and ureteral stents, are commonly used in the treatment and mitigation of urinary tract diseases, improving the patients' quality of life. However, the use of these devices is associated with serious complications, including the development of urinary tract infections (UTIs). UTIs account for 36 and 27% of the healthcare-associated infections reported in the United States and Europe, respectively [1,2], resulting in increased mortality rates and hospital costs [2–6]. Among hospital-acquired UTIs, 75% of cases have emerged from the insertion of urinary catheters (catheter-associated urinary tract infections) [7,8], and 31% from ureteral stents [9].

The insertion of these medical devices disturbs the local host defence mechanisms of patients, facilitating the access of microorganisms to the urinary tract and allowing their colonization [5].

Most UTDs are fabricated with silicone-based polymers such as poly(dimethylsiloxane) (PDMS) [10]. Despite its attractive properties, including the high mechanical and chemical stability and low toxicity, PDMS is extremely hydrophobic and, like the majority of the coating materials, is susceptible to bacteria and fungi adhesion [11,12]. In fact, UTDs are very prone to microbial adhesion and, consequently, biofilm formation, which is the leading cause for most UTIs. Different microorganisms have been identified as colonizers of UTDs, including *Escherichia coli*, *Staphylococcus aureus*, *Pseudomonas aeruginosa*, *Proteus* spp., *Klebsiella pneumoniae*, *Staphylococcus epidermidis*, *Enterococcus* spp. and *Candida* spp. [13,14]. Following microbial adhesion and colonization on UTD surfaces, microorganisms form biofilms, which protect them from the host immune system as well as from the action of antimicrobial agents, contributing to the persistence and spread of infection [15–17].

To date, different alternative materials with antimicrobial and antibiofilm properties have been developed to inhibit, or at least delay, biofilm formation. These strategies include the release of antimicrobial agents, contact-killing and anti-adhesive coatings, as well as surfaces that cause disruption of biofilm architecture by quorum sensing disturbance or matrix degradation [10]. However, although several preventive strategies having been proposed to reduce the incidence of UTIs, their application for coating UTDs is still questionable due to the resistance phenomena, low biocompatibility, and toxicity that derives from the use of some of these coatings [18].

In recent decades, carbon nanotubes (CNTs) have gained much attention in the industrial, environmental and biomedical fields. Described as sheets of graphene rolled up into cylinders (with several micrometres in length and nanometres in diameter), they can be classified as single- (SWCNTs) and multi-walled CNTs (MWCNTs), accordingly to the number of graphene layers [19,20]. Because of their outstanding properties, such as electrical conductivity, high aspect ratio and mechanical strength, flexibility, high surface energy density, chemical stability, and the possibility of functionalization with a wide variety of moieties (antimicrobial drugs and other bioactive molecules), CNT-based surfaces have been widely applied in the medical field, and in particular for the manufacture of medical devices [18,21]. Although there is still little consensus regarding the mechanisms behind the CNTs' antimicrobial activity, different influencing factors have been described, including CNT diameter and length, purity, electronic structure, CNT aggregation and surface functional groups, as well as CNT type (SWCNT or MWCNT) [22]. CNT activity is related not only to the mechanical damage (by the direct piercing of the microorganisms' outer membranes) and consequent cell disruption and release of intracellular content but also to the generation of oxidative stress [22].

Despite the proven antimicrobial activity of CNT composites [18,21], their application as a coating for urinary tract devices is still unexplored and supplementary investigations are required to improve their antimicrobial properties. To the best of our knowledge, only two studies have been devoted to the development of antimicrobial CNT composites for application in urinary tract devices in controlled hydrodynamic conditions [23,24]. In these studies, chemically and texturally modified MWCNT/PDMS composites efficiently modulated *E. coli* adhesion under conditions that mimic the urinary tract environment. However, there is a lack of knowledge about the efficacy of these composites in the prevention of biofilm formation under this specific context (hydrodynamic conditions, biological fluid, and temperature). Hence, the present study aimed to optimize MWCNT loading incorporated into a PDMS matrix and evaluate the performance of produced MWCNT/PDMS composites in preventing *E. coli* biofilm formation. Additionally, ball-milled CNT/PDMS composites were prepared as a strategy to evaluate the influence of CNTs dispersion pattern on the antimicrobial activity of the final composites.

2. Materials and Methods

2.1. Carbon Nanotubes

For the preparation of samples with different CNT loadings and milling times, commercially available pristine multi-walled CNTs (CNT-O, Nanocyl^{TM} NC3100, Sambreville, Belgium), produced by catalytic chemical vapor deposition with an average length and diameter of 1.5 µm and 9.5 nm, respectively, were used. According to data from the manufacturer, these CNTs only contain residual traces of growth catalyst impurities [25].

To produce CNT samples with different milling times, CNTs-O were physically modified by ball milling (BM) treatment. BM is a common technique used to adjust CNT length and open their closed ends, increasing their specific surface area [26]. Briefly, CNTs-O were submitted to BM treatment (Retsch MM200, Haan, Germany) at 15 vibrations s^{-1} for 1, 2, 3 and 4 h.

2.2. CNT/PDMS Composite Synthesis

The CNT/PDMS composites were produced through a bulk mixing process by directly incorporating CNT-O samples into the PDMS (Sylgard 184 Part A, Dow Corning, Midland, Michigan, USA; viscosity = 1.1 cm^2 s^{-1}; specific density = 1.03) matrix as described by Vagos et al. [23].

As the first aim of this study was to determine the most effective CNTs load to reduce bacterial biofilm formation, CNTs-O were incorporated in the PDMS matrix at 0.1, 1, 2, 3, 4 and 5% (wt%). These CNT loading values were chosen in line with previous results [23,24] that demonstrated a significant reduction in *E. coli* adhesion after incorporation of 0.1 and 1 wt% CNTs-O. Subsequently, in order to answer the second aim, 1, 2, 3 and 4 h ball-milled CNTs (CNT-BM 1 h; CNT-BM 2 h; CNT-BM 3 h and CNT-BM 4 h, respectively) were incorporated into the PDMS matrix at the optimal loading value to evaluate the effect of milling times in the CNTs antimicrobial properties. The ball-milling periods were selected based on the knowledge that CNTs surface area increases with increasing ball-milled periods between 1 and 4 h [26], increasing the chance for CNTs to interact and penetrate in the membranes of living bacteria [22].

The dispersion of CNT-O aggregates was first promoted by shear mixing with a magnetic bar at 500 rpm for 30 min and then using a sonication procedure (Hielscher UP400S, at 200 Watt and 12 kHz) for 1 h. The mixture was then placed in an ultrasound bath (Selecta Ultrasons, Lisbon, Tecnilab Portugal) for 30 min to eliminate residual air bubbles and the clusters of CNTs-O that remained. After that, the curing agent (Sylgard 184 Part B, Dow Corning, Midland, MI, USA) was added to the base-polymer (in an A:B proportion of 10:1) and carefully stirred to homogenize the two components without reintroducing bubbles. The composite materials were deposited as a thin layer (with a uniform thickness of 31 $\pm$ 3 µm) on top of glass slides through the spin coating technique (Spin150 Polos^{TM}, Caribbean, the Netherlands) at 6000 rpm for 1 min. Coated coupons were incubated overnight in an oven at 80 °C to induce the curing process. Bare PDMS surfaces (with a uniform thickness of 29 $\pm$ 3 µm) were also produced to be used as control.

2.3. Surface Characterization

2.3.1. Textural Properties

The evaluation of the textural properties of CNT samples (CNTs-O and CNT-BM) was based on the N_2 adsorption isotherms, determined at −196 °C with a Quantachrome NOVA 4200e multi-station apparatus (Quantachrome Instruments, Boynton Beach, USA). The surface areas of the CNT samples were determined according to the Brunauer–Emmett–Teller method (S_{BET}), and the total pore volume (V_p) was determined from the amount of N_2 uptake at a relative pressure close to unity, namely at p/p_0 = 0.99 [27]. The pore size distribution was calculated using the non-local density functional theory by applying the kernel file provided by Quantachrome's software, where a cylindrical-pore model is assumed.

2.3.2. Free Energy of Adhesion between Bacteria and Surfaces

The free energy of adhesion (ΔG_{iwI}^{TOT}) between the *E. coli* and all tested surfaces was assessed according to the procedure described by Gomes et al. [28]. Lawns of *E. coli* were prepared as described by Busscher et al. [29] in order to ascertain the bacterial surface hydrophobicity. Briefly, *E. coli* substrate was prepared by collecting bacterial cells from an overnight culture (grown under the conditions described in Section 2.4) on a cellulose membrane (pore diameter, 0.45 μm; Advantec, Tokyo, Japan) to a density of 1×10^8 cell mm^{-2}. Strips (with a width of 1 cm) were cut from the membranes and fixed onto a glass slide with double-sided adhesive tape for contact angle determination.

In the case of surfaces, the contact angle with water was determined before and after 24 h of exposure to sterile AUM, and very slight differences were observed (on average 4.4% reduction in surfaces exposed to the culture medium; Figure S1 of Supplementary Material).

The static contact angles of the bacteria and the surfaces were determined using the sessile drop technique (OCA 15 Plus, Dataphysics, Germany). The surface tension components of the bacteria and the adhesion surfaces were obtained by measuring the contact angles with three pure liquids. These measurements were carried out at room temperature (25 ± 2 °C) using water, formamide and α-bromonaphthalene (Sigma-Aldrich Co., St. Louis, MO, USA) as reference liquids (*I*). The surface tension components of the reference liquids were obtained from the literature [30]. Then, the hydrophobicity of the bacteria and the surfaces were evaluated by the method of van Oss et al. [31–33]. In this approach, the degree of hydrophobicity of a given material (*i*) is expressed as the free energy of interaction between two entities of that material immersed in water (*w*)—ΔG_{iwi}. If the interaction between the two entities is stronger than the interaction of each entity with water ($\Delta G_{iwi} < 0$ mJ m^{-2}), the material is considered hydrophobic. Conversely, if $\Delta G_{iwi} > 0$ mJ m^{-2}, the material is hydrophilic. ΔG_{iwi} was calculated from the surface tension components of the interacting entities, according to Equation (1):

$$\Delta G_{iwi} = -2\left(\sqrt{\gamma_i^{LW}} - \sqrt{\gamma_w^{LW}}\right)^2 + 4\left(\sqrt{\gamma_i^+\gamma_w^-} + \sqrt{\gamma_i^-\gamma_w^+} - \sqrt{\gamma_i^+\gamma_i^-} - \sqrt{\gamma_w^+\gamma_w^-}\right), \quad (1)$$

where γ^{LW} accounts for the Lifshitz–van der Waals component of the surface free energy and γ^+ and γ^- are the electron acceptor and electron donor parameters, respectively, of the Lewis acid-base component (γ^{AB}), with $\gamma^{AB} = 2\sqrt{\gamma^+\gamma^-}$.

The surface tension components were estimated by the simultaneous resolution of three equations of the type of Equation (2):

$$(1 + \cos\theta)\gamma_i^{TOT} = 2\left(\sqrt{\gamma_i^{LW}\gamma_I^{LW}} + \sqrt{\gamma_i^+\gamma_I^-} + \sqrt{\gamma_i^-\gamma_I^+}\right), \quad (2)$$

where θ is the contact angle and $\gamma^{TOT} = \gamma^{LW} + \gamma^{AB}$.

When studying the interaction (free energy of adhesion) between substances *i* and reference liquids *I* that are immersed or dissolved in water, the total interaction energy, ΔG_{iwI}^{TOT}, can be determined using Equation (3):

$$\Delta G_{iwI}^{TOT} = \gamma_{iI}^{LW} - \gamma_{iw}^{LW} - \gamma_{Iw}^{LW} + 2\left[\sqrt{\gamma_w^+}\left(\sqrt{\gamma_i^-} + \sqrt{\gamma_I^-} - \sqrt{\gamma_w^-}\right) + \sqrt{\gamma_w^-}\left(\sqrt{\gamma_i^+} + \sqrt{\gamma_I^+} - \sqrt{\gamma_w^+}\right) - \sqrt{\gamma_i^+\gamma_I^-} - \sqrt{\gamma_i^-\gamma_I^+}\right] \quad (3)$$

Thermodynamically, if $\Delta G_{iwI}^{TOT} < 0$ mJ m^{-2}, adhesion of the bacteria to the substratum is favourable, whereas adhesion is not favourable if $\Delta G_{iwI}^{TOT} > 0$ mJ m^{-2}.

2.3.3. Scanning Electron Microscopy (SEM)

The surface topology and the distribution of CNTs into the PDMS matrix were assessed by SEM. SEM analyses were performed using a high-resolution environmental scanning electron microscope with X-ray microanalysis and electron backscattered diffraction analysis (Quanta 400 FEG ESEM).

2.4. Bacterial Strain and Culture Conditions

E. coli CECT 434 expressing the green fluorescent protein (GFP) was used as a model pathogen to perform the antibiofilm assays. For the construction of *E. coli* CECT 434 GFP, the previously described pCM11 plasmid (Pmid19610092) carrying the gene encoding superfolder GFP (sGFP) and conferring ampicillin resistance was introduced in the CECT 434 strain by the heat shock method [34]. Besides this strain having a growth rate and biofilm formation capacity similar to the reference strain (*E. coli* CECT 434), it allows biofilms to be analysed by confocal microscopy without invasive sample preparation. The bacterial strain was preserved at −80 °C in Luria-Bertani Broth (Thermo Fisher Scientific, Waltham, MA, USA) containing 30% (*v/v*) glycerol, streaked on Plate Count Agar (PCA; Merck KGaA, Darmstadt, Germany) plates, and incubated for 24 h at 37 °C. Single colonies were collected from PCA plates, inoculated in 250 mL of artificial urine medium (AUM) [35] and incubated at 37 °C and 120 rpm for 16 ± 2 h to prepare a starting culture. Ampicillin at 0.1 g L^{-1} final concentration was used to maintain pCM11 in *E. coli* CECT 434. The overnight culture was centrifuged (Eppendorf Centrifuge 5810R, Hamburg, Germany) at 18 °C, 3772× *g* for 10 min, and resuspended in fresh AUM in order to obtain a final suspension with an optical density at 610 nm ($OD_{610\,nm}$) of 0.15. This $OD_{610\,nm}$ corresponds to approximately 1×10^8 colony-forming units per mL (CFU mL^{-1}), as confirmed by the retrospective count of CFUs.

2.5. Antibiofilm Assays

Antibiofilm assays were performed in 12-well microtiter plates (VWR International, Carnaxide, Portugal). Sterilized surfaces of PDMS, 0.1, 1, 2, 3, 4 and 5 wt% CNT-O/PDMS, and 3 wt% CNT/PDMS containing 1, 2, 3 and 4 h ball-milled CNTs were placed on the microplate wells and inoculated with 3 mL of *E. coli* suspension at a density of 1×10^8 cells mL^{-1}. Negative controls with 3 mL of AUM were prepared to evaluate the surface sterility throughout the experiments. Plates were incubated at 37 °C for 24 h under shaking conditions (100 rpm).

Biofilm formation assays were performed in three independent assays, each one with three technical replicates.

2.5.1. Biofilm Cell Quantification

After 24 h of biofilm formation, cell suspensions were obtained by dipping each surface in 2 mL 0.85% (*v/v*) NaCl and vortexing for 3 min. The number of biofilm culturable cells was assessed by spreading the biofilm suspension on PCA followed by manual counting of CFUs, while the biofilm total cell number was determined by staining the biofilm suspension with 4′-6-diamidino-2-phenylindole (Merck KGaA, Darmstadt, Germany) and analysing in an epifluorescence microscope (Leica DM LB2, Wetzlar, Germany) [28].

2.5.2. Confocal Laser Scanning Microscopy (CLSM)

To assess the biofilm spatial organization of the most promising surfaces, *E. coli* biofilms formed on PDMS, 3 wt% CNT-O/PDMS, 3 wt% CNT-BM 3 h/PDMS and 3 wt% CNT-BM 4 h/PDMS surfaces were observed using a 40× water objective (Leica HCX PL APO CS, Leica Microsystems, Wetzlar, Germany) in an inverted microscope Leica DMI6000-CS with a 488-nm argon laser. The emitted fluorescence was recorded within the range of 500 to 580 nm to collect the GFP emission fluorescence. A minimum of five stacks of horizontal plane images (512 × 512 pixels, corresponding to 387.5 µm × 387.5 µm) with a *z*-step of 1 µm were acquired for each biofilm sample.

Three-dimensional (3D) projections of biofilm structures were reconstructed from the CLSM acquisitions using the blend mode of the "Easy 3D" function of IMARIS 9.1 software (Bitplane, Zurich, Switzerland). The plug-in COMSTAT2 associated with the ImageJ software was used to determine the biovolume ($\mu m^3\ \mu m^{-2}$), biofilm thickness (µm) and surface coverage (%) [36].

2.6. Statistical Analysis

Descriptive statistics were used to calculate the mean and standard deviation or error for the number of culturable and total cells, biovolume, biofilm thickness and surface coverage. Differences between the number of culturable cells obtained for PDMS, 0.1, 1, 2, 3, 4 and 5 wt% CNT-O/PDMS, and 3 wt% CNT/PDMS surfaces containing 1, 2, 3 and 4 h ball-milled CNTs were evaluated using Kruskal-Wallis and Mann-Whitney tests since the variables were not normally distributed. For the number of total cells and quantitative CLSM analysis (biovolume, biofilm thickness and surface coverage), which were normally distributed, differences between the surfaces were determined using one-way analysis of variance followed by Tukey's multiple-comparison test.

Statistically significant differences were considered for p-values < 0.05 (corresponding to a confidence level greater than 95%; * and ** indicate $p < 0.01$ and $p < 0.001$, respectively).

Data analysis was performed using the IBM SPSS Statistics version 24.0 for Windows (IBM SPSS, Inc., Chicago, IL, USA).

3. Results and Discussion

3.1. CNTs Characterization

The characterization of ball-milled CNT samples is of particular importance since it is well known that particle morphology influences the porosity and the microstructure of the final composites [27]. The textural properties of CNT samples were evaluated by the N_2 adsorption–desorption isotherms for original and modified CNT samples (Figure 1).

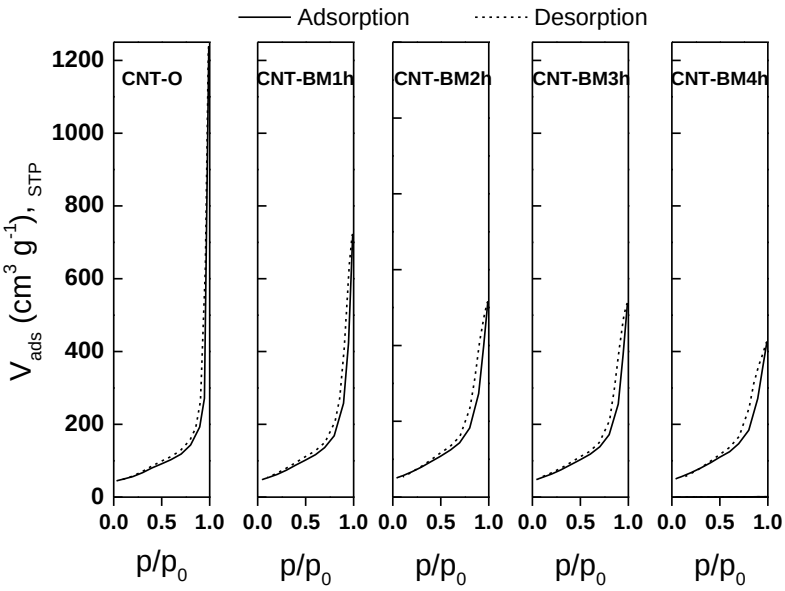

Figure 1. N_2 adsorption–desorption isotherms at −196 °C for pristine and modified carbon nanotubes (CNTs).

N_2 adsorption isotherms of original and ball-milled CNT samples were type IV isotherms (characteristic of carbon materials with some mesoporosity), according to IUPAC [37]. Despite the similarity between these isotherms, it is possible to notice a difference in the amount of N_2 adsorbed at high relative pressure, with lower amounts of N_2 adsorption for higher exposure periods to BM technique. These results are in accordance with previous studies, where the BM treatment by itself (4 h at a constant vibration frequency of 15 vibrations s^{-1}) induced a decrease of about 40% of N_2 adsorption at $p/p_0 = 0.95$ [38].

The results of N_2 adsorption–desorption isotherms are reflected in the specific surface area (S_{BET}) and total pore volume (V_p) of original and modified CNTs, represented in Table 1.

Table 1. Textural properties of pristine and modified CNTs.

Sample	S_{BET} (m^2 g^{-1})	$V_{p\ p/p0\ =\ 0.99}$ (cm^3 g^{-1})
CNT-O	197	1.917
CNT-BM 1 h	215	1.119
CNT-BM 2 h	219	0.825
CNT-BM 3 h	226	0.799
CNT-BM 4 h	227	0.661

From the results, it is possible to observe that BM treatment of CNTs resulted in an increase in the specific surface area compared to CNT-O. This phenomenon is already well-characterized and can be explained by the increase in the content of broken nanotubes and sidewall openings in the milled samples [39], which is in concordance with high-resolution transmission electron microscopy results reported elsewhere [40]. Taking into consideration that S_{BET} of CNT samples tends to be similar for milling times up to 1 h and to decrease for BM periods greater than 4 h (probably due to CNT compaction and twisting that limits the access of N_2 molecules to their inner part) [26], this work was limited to the study of CNT samples milled during 1, 2, 3 and 4 h. Although the S_{BET} of CNT-BM 4 h was higher than that of CNT-BM 1 h (227 and 215 m^2 g^{-1}, respectively), no relevant changes were observed with increasing exposure periods of CNTs to BM treatment (with differences within the experimental error). This is in accordance with N_2 adsorption isotherms at low relative pressure, where no major differences between samples were observed.

In addition to the changes in S_{BET}, a decrease in the V_p of ball-milled CNT samples was observed in comparison with CNT-O. This result can be explained by the differences in the degree of entanglement of CNTs, as the major part of the pore volume results from the space in CNT bundles [38]. During BM treatment, CNTs tend to compact and form larger agglomerates due to the collision of CNTs with the balls [26,41], thus decreasing the space between the tubes and, therefore, V_p. In fact, with increasing BM periods, a decrease was observed in the V_p, and the lowest value was obtained for 4 h ball-milled samples. According to previous studies, after this optimum value, the sample tends to present an opposite behaviour [26].

The pore size distribution (PSD), which is a measure of the distribution of pore volume concerning pore size (Figure 2), was also determined. The results obtained for ball-milled CNT samples showed significant changes in PSD compared to the original CNT sample. For the ball-milled samples, the number of pores with a half pore width higher than 80 Å is notably lower than the original sample. At the same time, new contributions were observed in the PSD of ball-milled CNTs for pore radius lower than 80 Å. The effect of BM treatment is even more evident for pore radius around 18–40 Å, where the sample CNT-BM 4 h presents larger peaks compared with the other ball-milled materials. This can be explained by the opening of CNT tips during the BM technique [39].

Altogether, these results suggest that the mechanical treatment induced in CNT samples was successful.

3.2. CNT/PDMS Characterization

The characterization of CNT/PDMS composites was initially performed through contact angle measurements and the calculation of the respective ΔG_{iwi} (Table 2). This last parameter is an indicator of the hydrophobicity of the sample, as previously explained (Section 2.3.2). From the final results, it is possible to observe that all the tested surfaces were hydrophobic, contrarily to *E. coli* CECT 434 GFP that demonstrated a hydrophilic character, similarly to previous studies with the same bacterial species [42].

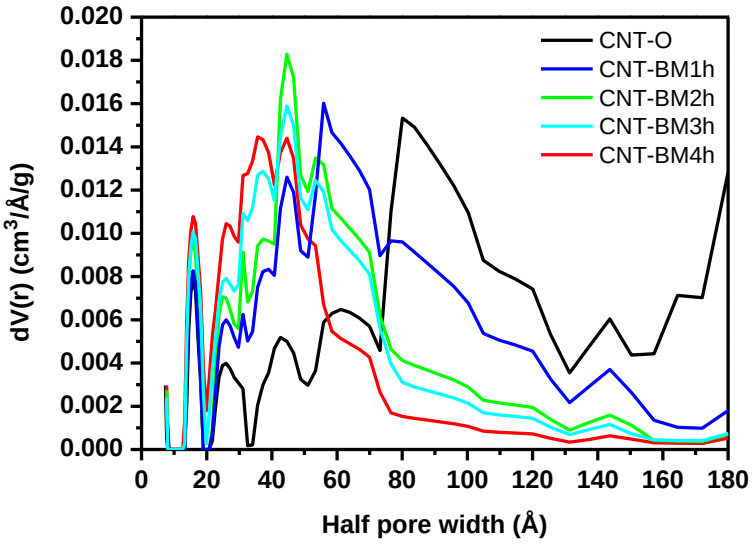

Figure 2. Pore size distributions obtained by Non-Linear Density Function Theory.

Table 2. Contact angles with water (θ_w), formamide (θ_F) and α-bromonaphthalene (θ_B), and free energy of interaction (ΔG_{iwi}) between two entities of a given material (i) (surface or bacteria) when immersed in water (w). Values are means ± standard deviations (SDs) of three independent experiments.

Sample	Contact Angle (°)			Hydrophobicity (mJ m^{-2})
	θ_w	θ_F	θ_B	ΔG_{iwi}
Surface				
PDMS	113.6 ± 1.7	111.2 ± 1.6	87.6 ± 6.1	−61.8
0.1 wt% CNT-O/PDMS	110.2 ± 1.0	101.3 ± 5.1	84.7 ± 1.8	−70.6
1 wt% CNT-O/PDMS	117.0 ± 2.4	110.4 ± 2.9	80.4 ± 2.5	−71.4
2 wt% CNT-O/PDMS	110.4 ± 1.9	104.5 ± 1.9	84.0 ± 3.8	−64.2
3 wt% CNT-O/PDMS	108.7 ± 2.4	105.9 ± 4.0	83.0 ± 2.8	−55.8
3 wt% CNT-BM 1 h/PDMS	107.9 ± 2.1	103.2 ± 2.5	81.5 ± 2.0	−58.3
3 wt% CNT-BM 2 h/PDMS	109.4 ± 1.8	104.9 ± 3.3	81.6 ± 3.5	−59.7
3 wt% CNT-BM 3 h/PDMS	114.8 ± 2.5	110.5 ± 2.9	88.7 ± 3.7	−67.5
3 wt% CNT-BM 4 h/PDMS	108.7 ± 2.0	106.7 ± 1.4	81.8 ± 1.9	−53.8
4 wt% CNT-O/PDMS	110.4 ± 3.0	104.0 ± 3.2	85.2 ± 3.1	−65.7
5 wt% CNT-O/PDMS	108.6 ± 2.2	105.6 ± 1.4	84.9 ± 2.7	−56.8
Bacteria				
E. coli CECT 434 GFP	19.4 ± 5.0	78.1 ± 5.5	62.2 ± 4.9	131.2

Looking a little closer, it is not possible to observe a linear trend in the evolution of hydrophobicity either with the incorporation of increasing CNT-O concentrations or with the use of ball-milled composites. Although only slight differences were obtained concerning the hydrophobicity of PDMS, it is interesting to note the lower hydrophobic character of 3 wt% CNT-O/PDMS and 3 wt% CNT-BM 4 h/PDMS surfaces. These surfaces presented, together with 3 wt% CNT-BM 1 h/PDMS and 5 wt% CNT-O/PDMS, lower values for the contact angle with water (with significant differences comparatively with PDMS and 1 wt% CNT-O/PDMS, $p < 0.01$).

As the free energy of adhesion (Table 3) is higher than 0 mJ m^{-2}, from a thermodynamic point of view, *E. coli* adhesion to PDMS and CNT/PDMS surfaces was not expected to occur. Following the same line of interpretation, it is also possible to state that 3 wt% CNT-O/PDMS, 3 wt% CNT-BM 4 h/PDMS and 5 wt% CNT-O/PDMS surfaces are less prone to microbial adhesion from a purely thermodynamic standpoint.

Table 3. Free energy of adhesion (ΔG_{iwl}^{TOT}) between *E. coli* CECT 434 GFP and the different surfaces when immersed in water (w).

Surface	ΔG_{iwl}^{TOT} (mJ m^{-2})
PDMS	37.7
0.1 wt% CNT-O/PDMS	31.9
1 wt% CNT-O/PDMS	30.9
2 wt% CNT-O/PDMS	35.0
3 wt% CNT-O/PDMS	39.0
3 wt% CNT-BM 1 h/PDMS	37.6
3 wt% CNT-BM 2 h/PDMS	36.9
3 wt% CNT-BM 3 h/PDMS	34.0
3 wt% CNT-BM 4 h/PDMS	39.9
4 wt% CNT-O/PDMS	34.4
5 wt% CNT-O/PDMS	38.8

Surface characterization of selected CNT-filled composites was complemented by SEM analysis (Figure 3). This microscopic technique allows the evaluation of the morphological details of materials at nanometre resolution, providing information regarding the degree of porosity and the presence of CNTs agglomerates.

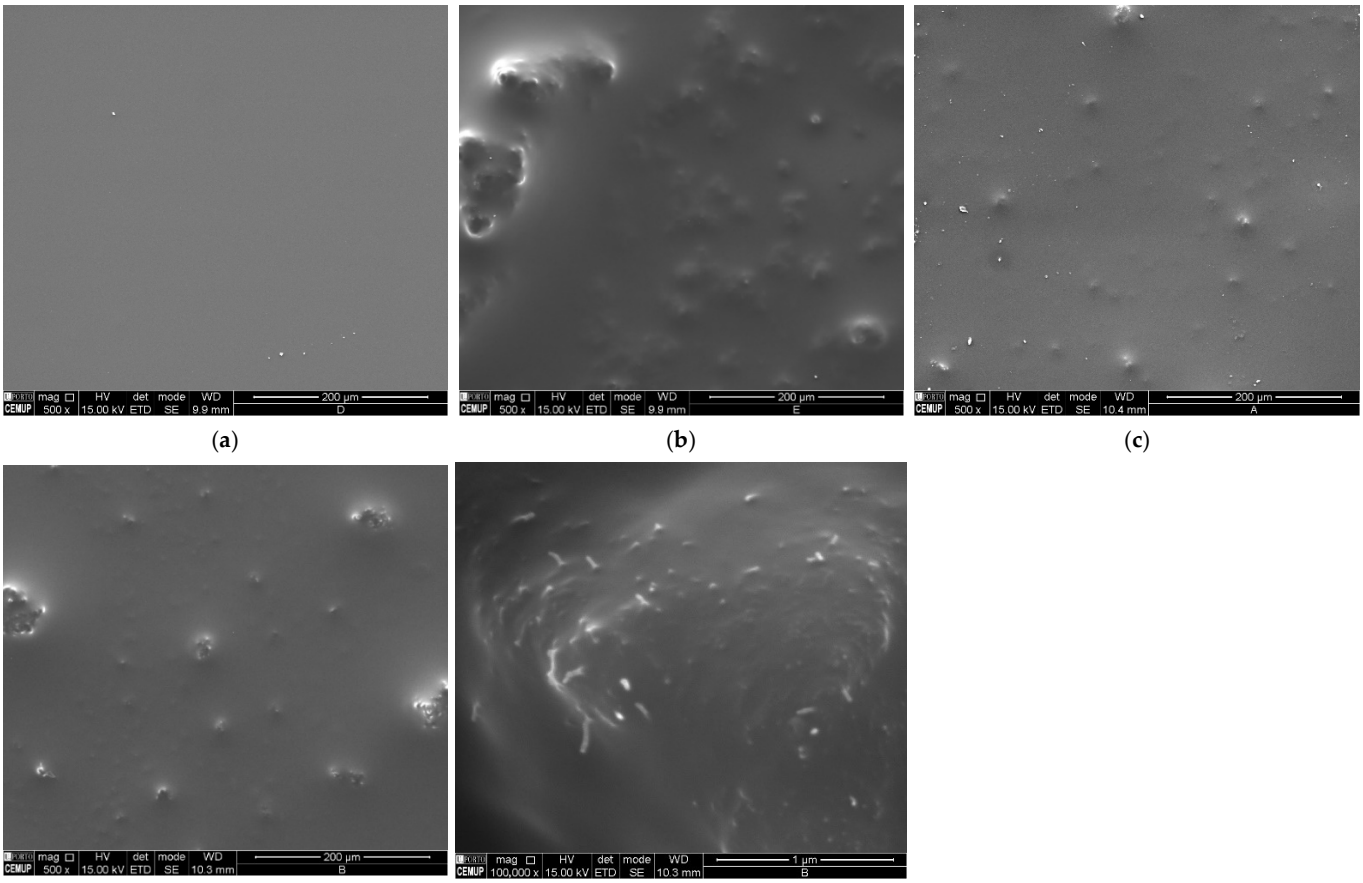

Figure 3. Scanning electron microscopy (SEM) images (magnification of 500×) of (**a**) poly(dimethylsiloxane) (PDMS); (**b**) 3 wt% CNT-O/PDMS; (**c**) 3 wt% CNT-BM 3 h/PDMS; and (**d**) 3 wt% CNT-BM 4 h/PDMS; (**e**) SEM image of 3 wt% CNT-BM 4 h/PDMS with a magnification of 100,000×.

From the observation of the SEM images, the presence of CNTs agglomerates forming small elevations in the surface of the composite is evident (Figure 3b–d). Additionally, dis-

tinct surface morphologies were detected. In fact, the improvement of CNT dispersion into the PDMS matrix is notorious after mechanical treatment by BM, particularly for 3 h ball-milled CNT/PDMS surfaces (Figure 3c), which is closely linked to CNT shortening [26,43].

On the other hand, when comparing 3 and 4 h ball-milled CNT/PDMS surfaces (Figure 3c,d), the latter showed an increment in the size of CNTs agglomerates, which can be explained by the increase of CNT compaction induced by the collision of CNTs with the balls during the dry BM process [26,41], as previously elucidated. Still, concerning the CNT-BM 4 h/PDMS surface, it was interesting to note some areas on the top of CNTs agglomerates where CNTs were more exposed (Figure 3e).

3.3. Antibiofilm Assays

To evaluate the influence of CNT-O loading in the antibiofilm activity of CNT-O/PMDS composites, a dynamic biofilm formation assay was performed with *E. coli* CECT 434 GFP. The results of culturable and total cells quantification after 24 h of incubation with 0.1, 1, 2, 3, 4 and 5 wt% CNT-O/PDMS composites are presented in Figure 4.

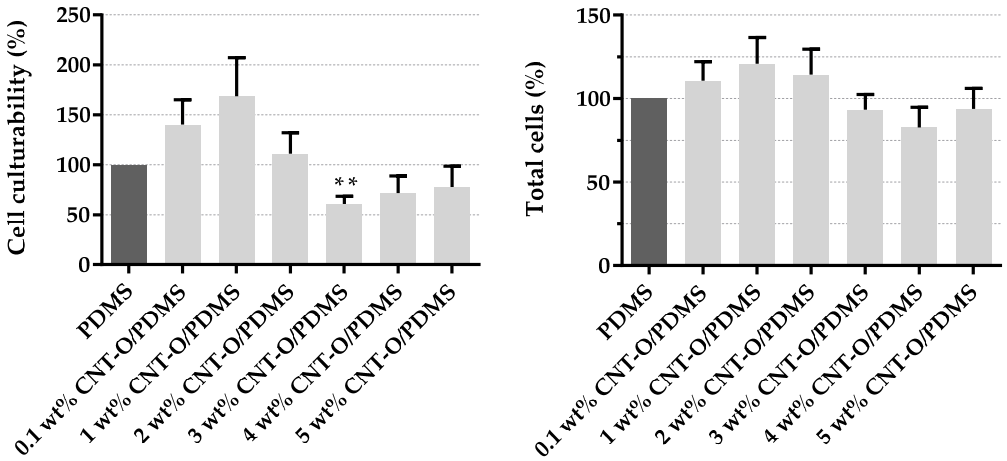

(**a**) (**b**)

Figure 4. Percentage of *E. coli* CECT 434 GFP (**a**) culturable and (**b**) total cells after 24 h of biofilm formation on PDMS (control) and CNT/PDMS composite surfaces with different CNT-O loading (ranging from 0.1 to 5 wt%). The means ± standard error (SE) for three independent experiments are illustrated. Significant differences were considered for *p*-values < 0.05 (** $p < 0.001$).

Despite the notorious increase in the percentage of culturable cells (Figure 4a) for surfaces with CNT loadings between 0.1 and 2 wt%, a decrease in those values was obtained for surfaces with higher CNT-O content. A total reduction of 39, 28 and 22% were achieved for 3, 4 and 5 wt% CNT-O/PDMS surfaces, respectively. However, only the surface with 3 wt% CNT-O loading presented a statistically significant reduction of cell culturability ($p < 0.001$), being the most promising surface for the inhibition of *E. coli* biofilms. The lower antimicrobial activity of 4 and 5 wt% CNT-O/PDMS surfaces may be justified by the decrease of CNTs dispersion degree imposed by increased loading, once the CNTs antimicrobial activity depends on their dispersion state [44]. Since no major differences were observed in the total cell number (Figure 4b), it is possible to assume that this decrease in cell culturability is a consequence of the antimicrobial activity of CNT-O/PDMS composites (an anti-adhesive activity would lead to a higher decrease in the total cell number). Indeed, an optimal CNT-O loading increases the availability of CNTs to interact with microbial cells on the matrix, without decreasing their dispersion degree, allowing CNTs to directly damage microbial membranes, with consequent cell death [22].

These results were corroborated by the contact angle measurements, where the introduction of distinct CNT-O concentrations only gave rise to slight changes in surface hydrophobicity.

After the initial optimization of the CNT-O loading, where the antimicrobial activity of 3 wt% CNT-O/PDMS composites against *E. coli* CECT 434 GFP stood out from the remaining surfaces, a new assay was performed in order to assess the influence of the CNTs dispersion pattern on the antimicrobial activity of the composites. In this particular case, PDMS matrices filled with 1, 2, 3 and 4 h ball-milled CNTs (at 3 wt%) were prepared. The results obtained for culturable and total cell counts are shown in Figure 5. After 24 h of biofilm growth, no significant reductions in the total cell number were observed. However, the number of culturable cells shows a statistically significant reduction in comparison to PDMS ($p < 0.001$). An average reduction of about 44% was obtained, indicating, once again, an antimicrobial effect against *E. coli* biofilms. A higher decrease in *E. coli* biofilm formation was achieved for the surfaces whose CNTs were ball-milled during 3 and 4 h (with a decrease of 54 and 53%, respectively, compared to PDMS).

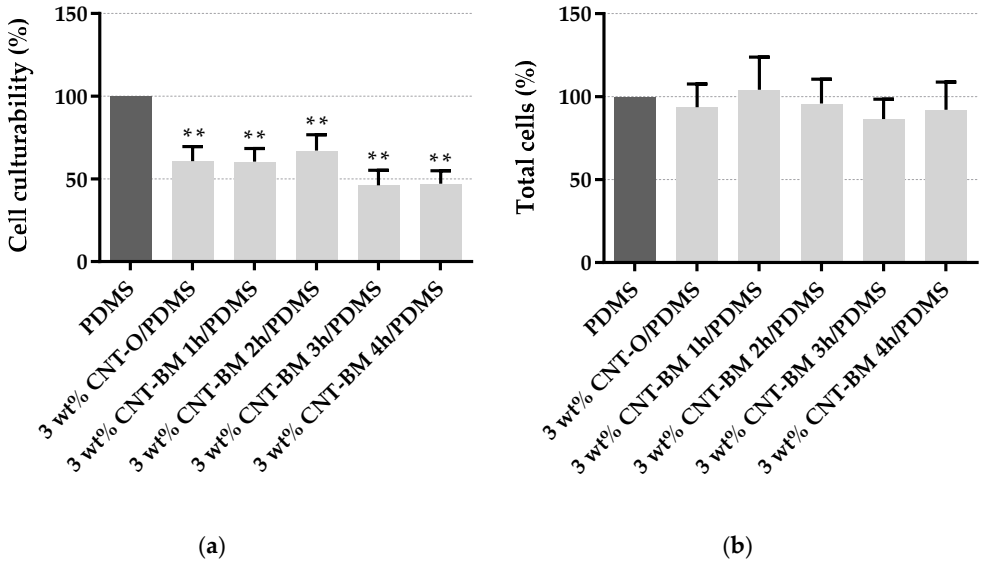

(**a**) (**b**)

Figure 5. Percentage of *E. coli* CECT 434 GFP (**a**) culturable and (**b**) total cells after 24 h of biofilm formation on PDMS (control), 3 wt% CNT-O/PDMS and 3 wt% CNT/PDMS composite surfaces containing 1, 2, 3 and 4 h ball-milled CNTs. The means ± SE for three independent experiments are illustrated. Significant differences were considered for *p*-values < 0.05 (** $p < 0.001$).

Results show a further decrease in the number of culturable cells for the ball-milled samples of around 24% when compared to the same loading (3 wt%) of CNT-O. This result suggests that BM treatment increases CNT's ability to disperse in the PDMS matrix, inducing morphological changes in the CNT/PDMS composites [45], which may increase the CNT surface contact with the microbial cells, leading to cell death [44]. Moreover, the effect of ball-milled CNTs on the reduction of *E. coli* adhesion and its association with the degree of dispersion of CNTs were already demonstrated [24].

Representative CLSM images of the *E. coli* CECT 434 GFP biofilms developed on the different surfaces (Figure 6) clearly show an effect of the BM treatment on biofilm architecture, while corroborating the cell quantification results obtained for 3 wt% CNT-O/PDMS composites. In fact, while PDMS surfaces were completely covered by dense biofilm, the presence of empty spaces on biofilm structure tends to increase with increasing BM regimes.

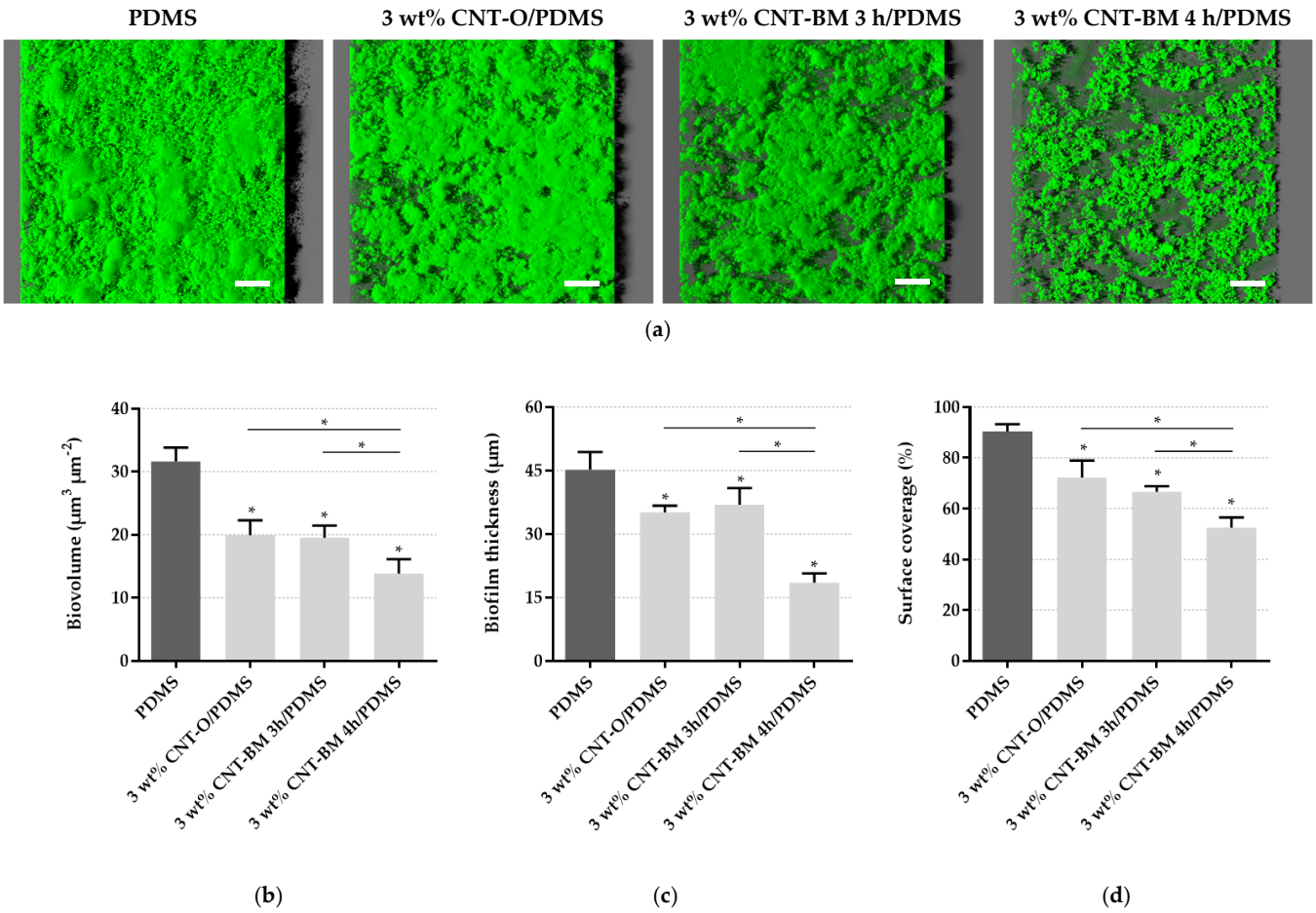

Figure 6. (**a**) Representative *E. coli* CECT 434 GFP biofilm structures on PDMS, 3 wt% CNT-O/PDMS, 3 wt% CNT-BM 3 h/PDMS and 3 wt% CNT-BM 4 h/PDMS. These images were obtained from confocal *z*-stacks using IMARIS software and present an aerial view of the biofilms (shadow projection on the right). The white scale bar corresponds to 50 μm. (**b**–**d**) Quantitative biofilm parameters obtained from the *z*-stacks: (**b**) biovolume, (**c**) thickness, and (**d**) surface coverage. The means ± SD for three independent experiments are illustrated. Significant differences were considered for *p*-values < 0.05 (* $p < 0.01$).

Although all the tested surfaces presented significant reductions in the three parameters analysed—biovolume, biofilm thickness and surface coverage—the 4 h ball-milled CNT/PDMS surface yielded the best results. In fact, when compared with 3 wt% CNT-O/PDMS, 4 h ball-milled CNTs composites reduced the amount of biofilm per surface area, biofilm thickness and surface coverage by 31, 47 and 27%, respectively. Although 4 h ball-milled CNT decreases the dispersion degree of CNTs into PDMS matrix compared to 3 h ball-milled CNT, the toxicity imposed by the presence of exposed CNTs on the surface of these particular composites, as demonstrated by SEM analysis (Figure 3e), may have increased their antimicrobial effect. In fact, by being more exposed, the piercing effect of CNTs on the membrane of bacterial cells [46,47] can be potentiated. Probably, by inducing a more open structure on the 3 wt% 4 h ball-milled CNT/PDMS composites, biofilms could be more susceptible to antimicrobial treatment [48], something that will be explored in future work.

Overall, these results suggest that CNTs dispersed into the PDMS matrix preserved their activity and increased microbial growth inhibition. Moreover, the use of polymers in the fabrication of CNT composites allows the conservation of structural and mechanical properties of the final composite in biological environments [49,50], limiting the release of CNTs and, consequently, their human toxicity.

4. Conclusions

Overall, this work demonstrated that the incorporation of a 3 wt% CNT-O loading into a PDMS matrix significantly reduced *E. coli* biofilm formation. Additionally, by ball-milling the original CNTs, an increase in the antibiofilm performance of these surfaces was achieved. Although only slight differences were observed between CNT-O and CNT-BM and their respective composites with PDMS (regarding the textural properties determined by N_2 adsorption isotherms and the hydrophobicity obtained by contact angle measurements), the results showed that 4 h ball-milled CNT/PDMS surfaces differ from the remaining surfaces in their morphology and have higher antibiofilm activity against *E. coli.*

Supplementary Materials: The following are available online at https://www.mdpi.com/article/10.3390/app11094038/s1, Figure S1: Water contact angles before (■) and after 24-h exposure (■) to artificial urine medium (AUM). Values are means ± standard deviations (SDs) of three independent experiments. Significant differences before and after medium exposure were considered for p-values < 0.05 (*).

Author Contributions: Conceptualization, M.F.R.P., O.S.G.P.S. and F.J.M.; methodology, M.G., L.C.G., R.T.-S., O.S.G.P.S.; investigation, M.G., L.C.G., R.T.-S., O.S.G.P.S.; resources, M.F.R.P. and F.J.M.; data curation, M.G., L.C.G., R.T.-S., O.S.G.P.S.; writing—original draft preparation, M.G., L.C.G., R.T.-S.; supervision, M.F.R.P., O.S.G.P.S. and F.J.M.; funding acquisition, M.F.R.P. and F.J.M. All authors have read and agreed to the published version of the manuscript.

Funding: This research was funded by: Base Funding—UIDB/50020/2020 of the Associate Laboratory LSRE-LCM—funded by national funds through FCT/MCTES (PIDDAC); Base Funding—UIDB/00511/2020 of the Laboratory for Process Engineering, Environment, Biotechnology and Energy—LEPABE—funded by national funds through the FCT/MCTES (PIDDAC); and by Project PTDC/CTM-COM/4844/2020 funded by FCT. R.T.-S. acknowledges the receipt of a junior researcher fellowship from the Project PTDC/BII-BIO/29589/2017—POCI-01-0145-FEDER-029589—funded by FEDER funds through COMPETE2020—Programa Operacional Competitividade e Internacionalização (POCI) and by national funds (PIDDAC) through FCT/MCTES. L.C.G. thanks the Portuguese Foundation for Science and Technology (FCT) for the financial support of her work contract through the Scientific Employment Stimulus—Individual Call—[CEECIND/01700/2017]. OSGPS acknowledges FCT funding under the Scientific Employment Stimulus—Institutional Call CEECINST/00049/2018.

Institutional Review Board Statement: Not applicable.

Informed Consent Statement: Not applicable.

Data Availability Statement: Not applicable.

Conflicts of Interest: The authors declare no conflict of interest.

References

1. European Centre for Disease Prevention and Control. *Annual Epidemiological Report on Communicable Diseases in Europe 2008*; European Centre for Disease Prevention and Control: Stockholm, Sweden, 2008.
2. Klevens, R.M.; Edwards, J.R.; Richards, C.L.; Horan, T.C.; Gaynes, R.P.; Pollock, D.A.; Cardo, D.M. Estimating health care-associated infections and deaths in U.S. hospitals, 2002. *Public Health Rep.* **2007**, *122*, 160–166. [CrossRef] [PubMed]
3. Foxman, B. Epidemiology of urinary tract infections: Incidence, morbidity, and economic costs. *Am. J. Med.* **2002**, *113*, 5–13. [CrossRef]
4. Scott, R.D., II. *The Direct Medical Costs of Healthcare-Associated Infections in the US Hospitals and the Benefits of Prevention*; Centers for Disease Control and Prevention: Atlanta, GA, USA, 2009.
5. Feneley, R.; Hopley, I.; Wells, P. Urinary catheters: History, current status, adverse events and research agenda. *J. Med. Eng. Technol.* **2015**, *39*, 459–470. [CrossRef]
6. Staubli, S.E.L.; Mordasini, L.; Engeler, D.S.; Sauter, R.; Schmid, H.-P.; Abt, D. Economic Aspects of Morbidity Caused by Ureteral Stents. *Urol. Int.* **2016**, *97*, 91–97. [CrossRef] [PubMed]
7. Zarb, P.; Coignard, B.; Griskeviciene, J.; Muller, A.; Vankerckhoven, V.; Weist, K.; Goossens, M.; Vaerenberg, S.; Hopkins, S.; Catry, B.; et al. The European Centre for Disease Prevention and Control (ECDC) pilot point prevalence survey of healthcare-associated infections and antimicrobial use. *Euro. Surveill.* **2012**, *17*, 20316–20331. [CrossRef] [PubMed]

8. Magill, S.S.; Edwards, J.R.; Bamberg, W.; Beldavs, Z.G.; Dumyati, G.; Kainer, M.A.; Lynfield, R.; Maloney, M.; McAllister-Hollod, L.; Nadle, J.; et al. Multistate point-prevalence survey of health care-associated infections. *N. Engl. J. Med.* **2014**, *370*, 1198–1208. [CrossRef]
9. Richter, S.; Ringel, A.; Shalev, M.; Nissenkorn, I. The indwelling ureteric stent: A 'friendly' procedure with unfriendly high morbidity. *BJU Int.* **2000**, *85*, 408–411. [CrossRef] [PubMed]
10. Gomes, M.; Gomes, L.C.; Teixeira-Santos, R.; Mergulhão, F.J. PDMS in Urinary Tract Devices: Applications, Problems and Potential Solutions. In *Polydimethylsiloxane: Structure and Applications*; Carlsen, P.N., Ed.; Nova Science Publishers: New York, NY, USA, 2020; pp. 95–144.
11. Souza, A.; Ribeiro, J.; Araújo, F. Study of PDMS characterization and its applications in biomedicine: A review. *J. Mech. Eng. Biomech.* **2019**, *4*, 1–9. [CrossRef]
12. Zhang, H.; Chiao, M. Anti-fouling Coatings of Poly(dimethylsiloxane) Devices for Biological and Biomedical Applications. *J. Med. Biol. Eng.* **2015**, *35*, 143–155. [CrossRef] [PubMed]
13. Maki, D.G.; Tambyah, P.A. Engineering out the risk for infection with urinary catheters. *Emerg. Infect. Dis.* **2001**, *7*, 342–347. [CrossRef] [PubMed]
14. Jacobsen, S.M.; Stickler, D.J.; Mobley, H.L.; Shirtliff, M.E. Complicated catheter-associated urinary tract infections due to *Escherichia coli* and *Proteus mirabilis*. *Clin. Microbiol. Rev.* **2008**, *21*, 26–59. [CrossRef] [PubMed]
15. Anjum, S.; Singh, S.; Benedicte, L.; Roger, P.; Panigrahi, M.; Gupta, B. Biomodification Strategies for the Development of Antimicrobial Urinary Catheters: Overview and Advances. *Glob. Chall.* **2018**, *2*, 1700068–1700081. [CrossRef]
16. Ramstedt, M.; Ribeiro, I.A.C.; Bujdakova, H.; Mergulhão, F.J.M.; Jordao, L.; Thomsen, P.; Alm, M.; Burmølle, M.; Vladkova, T.; Can, F.; et al. Evaluating Efficacy of Antimicrobial and Antifouling Materials for Urinary Tract Medical Devices: Challenges and Recommendations. *Macromol. Biosci.* **2019**, *19*, 1800384–1800409. [CrossRef] [PubMed]
17. Zhu, Z.; Wang, Z.; Li, S.; Yuan, X. Antimicrobial strategies for urinary catheters. *J. Biomed. Mater. Res. A* **2019**, *107*, 445–467. [CrossRef]
18. Teixeira-Santos, R.; Gomes, M.; Gomes, L.C.; Mergulhão, F.J. Antimicrobial and anti-adhesive properties of carbon nanotube-based surfaces for medical applications: A systematic review. *iScience* **2021**, *24*, 102001–102024. [CrossRef] [PubMed]
19. Upadhyayula, V.K.; Gadhamshetty, V. Appreciating the role of carbon nanotube composites in preventing biofouling and promoting biofilms on material surfaces in environmental engineering: A review. *Biotechnol. Adv.* **2010**, *28*, 802–816. [CrossRef] [PubMed]
20. Veetil, J.V.; Ye, K. Tailored carbon nanotubes for tissue engineering applications. *Biotechnol. Prog.* **2009**, *25*, 709–721. [CrossRef]
21. Teixeira-Santos, R.; Gomes, M.; Mergulhão, F.J. Carbon Nanotube-Based Antimicrobial and Antifouling Surfaces. In *Engineered Antimicrobial Surfaces. Materials Horizons: From Nature to Nanomaterials*; Snigdha, S., Thomas, S., Radhakrishnan, E., Kalarikkal, N., Eds.; Springer: Singapore, 2020; pp. 65–93.
22. Kang, S.; Herzberg, M.; Rodrigues, D.F.; Elimelech, M. Antibacterial Effects of Carbon Nanotubes: Size Does Matter! *Langmuir* **2008**, *24*, 6409–6413. [CrossRef]
23. Vagos, M.R.; Moreira, J.M.R.; Soares, O.S.G.P.; Pereira, M.F.R.; Mergulhao, F.J. Incorporation of Carbon Nanotubes in Polydimethylsiloxane to Control *Escherichia coli* Adhesion. *Polym. Compos.* **2019**, *40*, 1697–1704. [CrossRef]
24. Vagos, M.R.; Gomes, M.; Moreira, J.M.R.; Soares, O.S.G.P.; Pereira, M.F.R.; Mergulhão, F.J. Carbon Nanotube/Poly(dimethylsiloxane) Composite Materials to Reduce Bacterial Adhesion. *Antibiotics* **2020**, *9*, 434. [CrossRef] [PubMed]
25. Gonçalves, A.G.; Figueiredo, J.L.; Órfão, J.J.M.; Pereira, M.F.R. Influence of the surface chemistry of multi-walled carbon nanotubes on their activity as ozonation catalysts. *Carbon* **2010**, *48*, 4369–4381. [CrossRef]
26. Soares, O.S.G.P.; Gonçalves, A.G.; Delgado, J.J.; Órfão, J.J.M.; Pereira, M.F.R. Modification of carbon nanotubes by ball-milling to be used as ozonation catalysts. *Catal. Today* **2015**, *249*, 199–203. [CrossRef]
27. Rocha, R.P.; Silva, A.M.T.; Romero, S.M.M.; Pereira, M.F.R.; Figueiredo, J.L. The role of O- and S-containing surface groups on carbon nanotubes for the elimination of organic pollutants by catalytic wet air oxidation. *Appl. Catal. B* **2014**, *147*, 314–321. [CrossRef]
28. Gomes, L.C.; Silva, L.N.; Simões, M.; Melo, L.F.; Mergulhão, F.J. *Escherichia coli* adhesion, biofilm development and antibiotic susceptibility on biomedical materials. *J. Biomed. Mater. Res. Part A* **2015**, *103*, 1414–1423. [CrossRef] [PubMed]
29. Busscher, H.J.; Weerkamp, A.H.; van der Mei, H.C.; van Pelt, A.W.; de Jong, H.P.; Arends, J. Measurement of the surface free energy of bacterial cell surfaces and its relevance for adhesion. *Appl. Environ. Microbiol.* **1984**, *48*, 980–983. [CrossRef] [PubMed]
30. Janczuk, B.; Chibowski, E.; Bruque, J.M.; Kerkeb, M.L.; Caballero, F.G. On the Consistency of Surface Free Energy Components as Calculated from Contact Angles of Different Liquids: An Application to the Cholesterol Surface. *J. Colloid Interface Sci.* **1993**, *159*, 421–428. [CrossRef]
31. Van Oss, C.J.; Chaudhury, M.K.; Good, R.J. Monopolar surfaces. *Adv. Colloid Interface Sci.* **1987**, *28*, 35–64. [CrossRef]
32. Van Oss, C.J.; Good, R.J.; Chaudhury, M.K. Additive and nonadditive surface tension components and the interpretation of contact angles. *Langmuir* **1988**, *4*, 884–891. [CrossRef]
33. Van Oss, C.J.; Ju, L.; Chaudhury, M.K.; Good, R.J. Estimation of the polar parameters of the surface tension of liquids by contact angle measurements on gels. *J. Colloid Interface Sci.* **1989**, *128*, 313–319. [CrossRef]
34. Sambrook, J.; Fritsch, E.F.; Maniatis, T. *Molecular Cloning: A Laboratory Manual*; Cold Spring Harbor Laboratory: Huntington, NY, USA, 1989.

35. Brooks, T.; Keevil, C.W. A simple artificial urine for the growth of urinary pathogens. *Lett. Appl. Microbiol.* **1997**, *24*, 203–206. [CrossRef]
36. Heydorn, A.; Nielsen, A.T.; Hentzer, M.; Sternberg, C.; Givskov, M.; Ersbøll, B.K.; Molin, S. Quantification of biofilm structures by the novel computer program comstat. *Microbiology* **2000**, *146*, 2395–2407. [CrossRef]
37. Sing, K. Reporting Physisorption Data for Gas/Solid Systems with Special Reference to the Determination of Surface Area and Porosity. *Pure Appl. Chem.* **1982**, *54*, 2201–2218. [CrossRef]
38. Rocha, R.P.; Soares, O.S.G.P.; Gonçalves, A.G.; Órfão, J.J.M.; Pereira, M.F.R.; Figueiredo, J.L. Different methodologies for synthesis of nitrogen doped carbon nanotubes and their use in catalytic wet air oxidation. *Appl. Catal. A* **2017**, *548*, 62–70. [CrossRef]
39. Soares, O.S.G.P.; Rocha, R.P.; Gonçalves, A.G.; Figueiredo, J.L.; Órfão, J.J.M.; Pereira, M.F.R. Easy method to prepare N-doped carbon nanotubes by ball milling. *Carbon* **2015**, *91*, 114–121. [CrossRef]
40. Kónya, Z.; Zhu, J.; Niesz, K.; Mehn, D.; Kiricsi, I. End morphology of ball milled carbon nanotubes. *Carbon* **2004**, *42*, 2001–2008. [CrossRef]
41. Ahn, J.H.; Shin, H.S.; Kim, Y.J.; Chung, H. Structural modification of carbon nanotubes by various ball milling. *J. Alloys Compd.* **2007**, *434*, 428–432. [CrossRef]
42. Moreira, J.M.R.; Ponmozhi, J.; Campos, J.B.L.M.; Miranda, J.M.; Mergulhão, F.J. Micro- and macro-flow systems to study *Escherichia coli* adhesion to biomedical materials. *Chem. Eng. Sci.* **2015**, *126*, 440–445. [CrossRef]
43. Ma, P.-C.; Siddiqui, N.A.; Marom, G.; Kim, J.-K. Dispersion and functionalization of carbon nanotubes for polymer-based nanocomposites: A review. *Compos. Part A Appl. Sci. Manuf.* **2010**, *41*, 1345–1367. [CrossRef]
44. Saleemi, M.A.; Fouladi, M.H.; Yong, P.V.C.; Wong, E.H. Elucidation of Antimicrobial Activity of Non-Covalently Dispersed Carbon Nanotubes. *Materials* **2020**, *13*, 1676. [CrossRef]
45. Tucho, W.M.; Mauroy, H.; Walmsley, J.C.; Deledda, S.; Holmestad, R.; Hauback, B.C. The effects of ball milling intensity on morphology of multiwall carbon nanotubes. *Scr. Mater.* **2010**, *63*, 637–640. [CrossRef]
46. Chen, H.; Wang, B.; Gao, D.; Guan, M.; Zheng, L.; Ouyang, H.; Chai, Z.; Zhao, Y.; Feng, W. Broad-spectrum antibacterial activity of carbon nanotubes to human gut bacteria. *Small* **2013**, *9*, 2735–2746. [CrossRef] [PubMed]
47. Kang, S.; Pinault, M.; Pfefferle, L.D.; Elimelech, M. Single-Walled Carbon Nanotubes Exhibit Strong Antimicrobial Activity. *Langmuir* **2007**, *23*, 8670–8673. [CrossRef] [PubMed]
48. Alves, P.; Gomes, L.C.; Rodríguez-Emmenegger, C.; Mergulhão, F.J. Efficacy of A Poly(MeOEGMA) Brush on the Prevention of *Escherichia coli* Biofilm Formation and Susceptibility. *Antibiotics* **2020**, *9*, 216. [CrossRef] [PubMed]
49. Aslan, S.; Loebick, C.Z.; Kang, S.; Elimelech, M.; Pfefferle, L.D.; Van Tassel, P.R. Antimicrobial biomaterials based on carbon nanotubes dispersed in poly(lactic-co-glycolic acid). *Nanoscale* **2010**, *2*, 1789–1794. [CrossRef] [PubMed]
50. Liu, Z.; Sun, X.; Nakayama-Ratchford, N.; Dai, H. Supramolecular Chemistry on Water-Soluble Carbon Nanotubes for Drug Loading and Delivery. *ACS Nano* **2007**, *1*, 50–56. [CrossRef] [PubMed]